Influence of debinding and sintering conditions on the composition and thermal conductivity of copper parts printed from highly loaded photocurable formulations

Marilyne Roumanie, Cecile Flassayer, Adrien Resch, Laurent Cortella, Richard Laucournet

Research Article

Influence of debinding and sintering conditions on the composition and thermal conductivity of copper parts printed from highly loaded photocurable formulations

Marilyne Roumanie[1,2] · Cécile Flassayer[1,2] · Adrien Resch[1,2] · Laurent Cortella[3] · Richard Laucournet[1,2]

Received: 14 September 2020 / Accepted: 22 December 2020

Abstract
Metal 3D printing based on the photopolymerization reaction (Digital Light Processing—DLP) of an organic matrix in which metal particles are embedded is a developing technology. This technology requires a step of resin removal and densification by sintering to obtain a metal part. This process has been applied to copper. Photocurable formulations with a high loading rate of copper powder of 60 vol.% were developed and suitable for DLP printing with thicknesses > 25 µm. Debinding and sintering cycles were investigated on specimens fast cured by gamma irradiation to save materials and time. A debinding in air at 400 °C and sintering in hydrogen lead to a C content of 0.018 wt.%, similar to the raw copper powder and slightly higher oxygen content. The low thermal conductivity of 250 $W \cdot m^{-1} \cdot K^{-1}$ highlighted the harmful effect of phosphorus from the powder and photoinitiators such as BAPO. The C and O contents and the thermal conductivity measured on copper parts printed by DLP confirm the results obtained on specimens cured by gamma irradiation.

Keywords Digital light processing · Copper · Impurities · Additive manufacturing · Gamma irradiation · Stereolithography

1 Introduction

Copper exhibits high thermal and electrical performances, antibacterial properties and is easy to recycle [1]. These properties make copper excellent material for solar and wind energy, power electronics, medical, or telecommunication [2, 3]. New designs reachable with additive manufacturing are required to improve the performance of power generators or antennas.

Digital Light Processing (DLP) technology, based on the photopolymerization reaction of a resin, is known for the printing of polymer [4–6] and ceramic objects [7–9] and is being developed for metal structures [10–14]. The process of manufacturing a metal part using this printing technology includes four steps like for ceramics. The first step consists of formulating a printing material suitable for DLP technology in terms of cured thickness (> 25 µm) and loading rate (> 45 vol.%) to obtain a dense object at the end of the process. This printing material contains a mixture of monomers and/or oligomers acrylates with photoinitiator and metal particles. Metals are known to absorb UV light, making it difficult to combine high cured thicknesses with a high loading rate. The second step is to print this material layer by layer. The photoinitiator in the formulation decomposes into reactive species under UV light. These reactive species interact with the acrylate functions to form a cured three-dimensional network. The organic network is a thermoset material with good mechanical strength, infusible, and insoluble. Metallic particles become trapped in this organic network. Once the object is printed, the resin is removed by thermal debinding to obtain a metal part. The debinding atmospheres

✉ Marilyne Roumanie, marilyne.roumanie@cea.fr | [1]Université Grenoble Alpes, 38000 Grenoble, France. [2]CEA-LITEN, 17 rue des Martyrs, 38054 Grenoble, France. [3]ARC-Nucléart, CEA Grenoble, 17 rue des Martyrs, 38054 Grenoble, France.

Published online: 10 January 2021

are generally reducing, neutral, or vacuum atmospheres to avoid metal oxidation and lower the parts' mechanical properties. Under these conditions, the organic network could be partially burned out, and the material health can be impacted. Finally, the part is consolidated by sintering to obtain a dense metal part.

In 2006, Lee et al. [10] published the feasibility of printing green copper parts by DLP and obtain copper structures after debinding and sintering. The layers are printed with thicknesses suitable for DLP machines, i.e., greater than 25 µm and a low copper loading of 30 vol.%. The object's electrical resistivity is between 200 and 300 nΩ·m, more than ten times higher than that of pure copper (16.78 nΩ·m [15]). The authors attribute this difference to the presence of porosity in the copper part. However, the copper presents a dark red color, resulting from oxidation of the material or impurities due to the high content of organic resin, which could be partially burned out in argon. No details regarding the chemical composition are reported.

In 2009, Kirihara et al. [13, 14] published copper photonic crystals printed by micro-SLA. The photosensitive formulation includes a high copper loading of 54 vol.%. The cured thicknesses are, however, low of 10 µm. These conditions permit to print of objects with a high resolution of 2 µm, adapted to the targeted applications. Again no details on the final composition are mentioned.

This work's first objective is to develop photosensitive formulations with a high loading of copper particles (> 45 vol.%) suitable for DLP printing technology, i.e., with layer thicknesses > 25 µm. The second one is to investigate the copper parts' final composition and properties, such as thermal conductivity according to the developed formulations and the thermal conditions of debinding/sintering. This investigation requires a large number of samples, time, i.e., to set up the machine parameters and, consequently, a high quantity of material. The approach is based on gamma irradiation curing to save time and material. Among irradiation technology by ionizing radiation, gamma irradiation has unrivaled penetrating power. Gamma irradiation cures monomer and oligomer acrylates [16, 17], polymers included in the formulation for 3D printing by DLP. It enables us to cure several formulations poured in tubes with a unique dose at one go. This approach is finally compared to the chemical composition and thermal properties of objects printed by DLP and then debinded and sintered regarding the conditions determined on the gamma-ray cured samples.

2 Materials and methods

2.1 Copper photocurable formulations

2.1.1 Photocurable resins

Four photocurable resins noted F1, F2, F3, and F4 were studied and described in Table 1.

The composition of the resin F1 is a blend of 1,6-hexanediol diacrylate (SR238-Sartomer), tetrafunctionnal oligoacrylate (SR355-Sartomer), and an amine-modified polyether acrylate (CN509-Sartomer). A part of the CN509 was replaced in the formulation F2 by the polyester acrylate (CN371EU-Sartomer). The polyester acrylate allows to burn out the resin on a wide range of temperatures that could limit cracks during the copper parts' debinding stage. In F3 and F4 formulations, CN509 and CN371 were replaced by the ethoxylated bisphenol A dimetacrylate (Diacryl 101), usually used in photocurable ceramic formulations [18, 19].

MMMP (2-methyl-4′-methylthio-2-morpholinopropiophenone-Sigma Aldrich), photoinitiator (PI) known for its high reactivity and BAPO (Phenylbis (2,4,6-trimethyl-benzoyl)phosphine oxide-Sigma Aldrich), having a photobleaching behavior are dissolved by magnetic stirring in F1, F2, and F3 resins. DMPA (2,2-dimethoxy-2-phenyl acetophenone) photoinitiator is dissolved in F4 resin. PI rate is fixed at 5 wt.% by a photocurable fraction.

The photocurable resin amounts to 40 vol.% in the copper formulation.

2.1.2 Copper

Commercial air atomized copper powder supplied by ECKA Granules® was used as loading material in the photocurable formulation. Figure 1a shows a Scanning Electron Microscopy (SEM) image of the as-received spherical

Table 1 Composition of the photocurable resins

	Acrylates	Photoinitiators		
			wt.%	mol L^{-1}
F1	SR355, SR238, CN509	BAPO/MMMP	2.5/2.5	$5.9\times10^{-2}/8.9\times10^{-2}$
F2	SR355, SR238, CN509, CN371	BAPO/MMMP	2.5/2.5	$5.9\times10^{-2}/8.9\times10^{-2}$
F3	SR355, SR238, Diacryl 101	BAPO/MMMP	2.5/2.5	$5.9\times10^{-2}/8.9\times10^{-2}$
F4	SR355, SR238, Diacryl 101	DMPA	5	19.5×10^{-2}

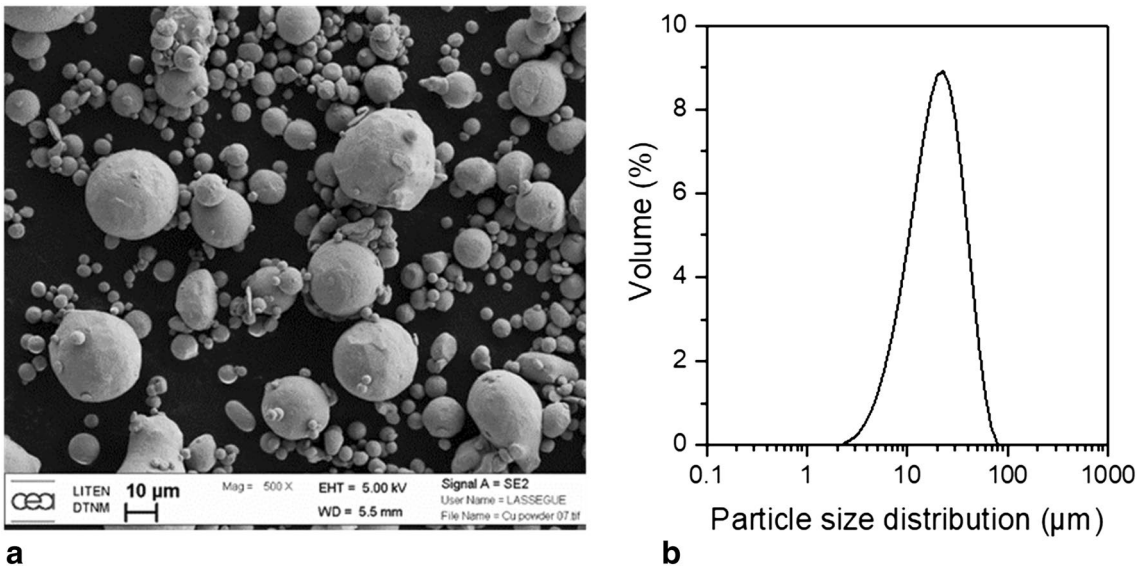

Fig. 1 Copper Ecka powder **a** observation by SEM **b** particle size distribution in volume

Table 2 Powder batch as specified by ICP-OES and oxygen measurement (ECKA Granules® data)

Element	Cu	B	P	C	N	O	H
Mass fraction (wt.%)	> 99.9	0.01	0.02	0.02	< 0.05	< 0.05	< 0.05

copper powder. The copper powder consists of a monomodal volume distribution (DV) with a DV(50) of 22 µm and a DV(90) of 42 µm (Fig. 1b; laser MS2000 granulometry-Malvern Instruments). The copper chemical analysis is reported in Table 2 shows a purity below 99.9% with 0.02 wt.% of phosphorus. The copper powder is considered as a Deoxidized High Phosphorus (DHP) copper (Cu ≥ 99.90 and 0.013–0.05 wt.% P).

2.2 Curing routes

2.2.1 Curing by UV

The curing behavior of copper formulations is determined by measuring the cured layer thickness with the exposure time at a wavelength of 365 nm and an irradiance of 88 mW·cm^{-2}. A layer of a copper formulation is spread on a glass substrate by a blade. An emitting UV device lights a square pattern onto the spread layer during 1, 2, and 5 s, corresponding to energies of 88, 176, and 440 mJ·cm^{-2}, respectively. The cured layer thickness is measured with a digital micrometer. As the DLP is a layer-wise printing process, sufficient energy is required to cure the printed layer and bond the layer with the previously cured layer. The minimum cured thickness layer, to assess if the curing behavior is suitable for printing, is fixed at 50 µm. Therefore the minimum printing layer is 25 µm.

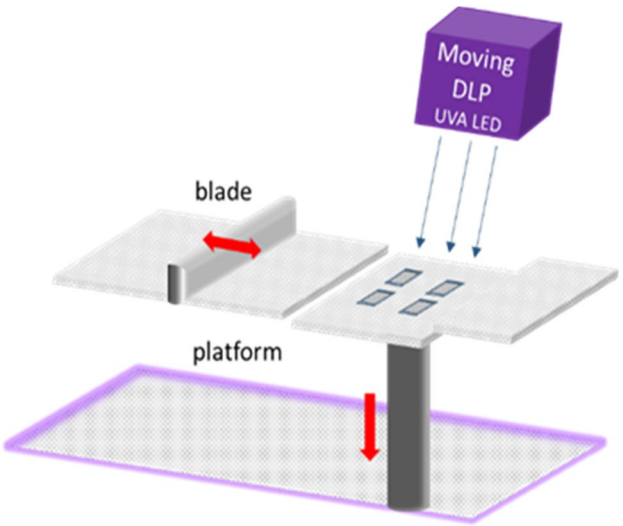

Fig. 2 DLP operating equipment

Copper printing is conducted on a photocurable copper formulation using Digital Light Processing equipment (ProMaker V6000 - Prodways). The operating principle is described in Fig. 2. The printing approach is top-down as

the DLP source is positioned above the printing platform. As the copper density is high (8.9 g·cm^{-3} [20]) to limit the particle settling, the high viscosity of the formulation is required (above 10 Pa·s at a shear rate of 100 s^{-1}). The feeder system delivers a volume of paste onto the platform, which is spread in thin layers (25–100 µm) with a dual-blade system. The UV head (Wavelength 365 nm - Irradiance 88 mW·cm^{-2}) lights a pattern of the layer of the part to be printed. Upon photocured, the platform moves down a height of a layer. A new layer of paste is spread on top of the previous one, and the process is carried on until the 3D part is entirely built.

2.2.2 Curing by gamma irradiation

An intermediate pool research irradiator was used in this study. It is a straightforward but exciting tool, offering high-intensity radiation and adapted to many geometric configurations. Cobalt 60 (^{60}Co) radioactive standard industrial sources are used, delivering 1.17 and 1.33 MeV photons for each beta disintegration.

Figure 3 describes the principle of the pool irradiation process in ARC-Nucléart, Grenoble, France. The irradiator consists of a 4.25 m deep water pool in which radioactive sources are stored, water assuring the protection of operators against the gamma irradiation. The sources, currently divided into 20 ^{60}Co sources from 10 to 300 TBq, are mounted on a mobile track connected to the pool via a channel that passes through the base of the chamber's wall. The sources can be thus transferred from the pool to the irradiation chamber. Inside the irradiation chamber, in the current track configuration, a dose rate of approximately 2 kGy·h^{-1} or above is typically obtained at a distance of 10 cm from the source rack.

For fast curing out of the DLP printer, copper formulations are poured into tubes and cured by gamma irradiation at a dose of 30 kGy in 15–20 h. Then, green copper specimens are sliced in cylinders with 5 mm height and 13 mm diameter.

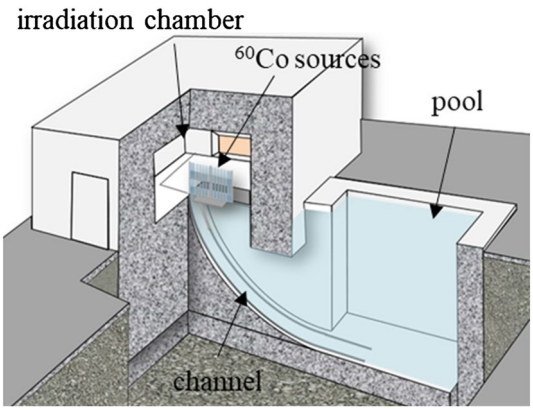

Fig. 3 Principle diagram of the pool irradiation process

2.3 Thermal cycling

Final carbon and oxygen contents, and therefore, the purity and the properties of final sintered parts are closely correlated to the composition of photocurable resins and the debinding stage. The thermal process was performed on specimens cured by gamma irradiation to optimize the debinding parameters according to copper formulations. The debinding cycles were conducted in hydrogen from room to debinding temperature, using different debinding temperatures (400, 600, and 800 °C), different dwell times (4, 7, and 10 h), and different partial pressures (50, 400, and 600 mbar). Different debinding atmospheres (air, vacuum, argon, 600 ppm, and 5 wt.% of oxygen in argon) were studied as well at a debinding temperature of 400 °C during 4 h. Finally, the copper specimens are naturally cooled to room temperature.

Debinded gamma-ray specimens and DLP printed parts were sintered in a hydrogen atmosphere at three temperature dwells 980, 1030, and 1050 °C, a constant heating rate of 3 °C·min^{-1}, and partial pressure of 400 mbar during 4 h. The hydrogen atmosphere reduces the oxygen in the copper powder and makes the copper densification easier.

2.4 Characterizations

The total reflectivity of copper powder is measured using a laser spectrophotometer (Lambda 950 Perkin Elmer) coupled to an integrating sphere from a quartz cell filled with copper. The measuring wavelength range is between 250 and 500 nm with a 5 nm step. The optical path cell is 1 cm. No transmission is measured in such a condition. The absorption is then calculated from the following Eq. (1):

$$A\% = 100\% - R\% \quad (1)$$

where A [%] is the absorption, and R [%] is the total reflectivity.

Resin degradation was determined using thermogravimetric analysis (TGA Netzsch STA 449) in argon and air atmospheres at a heating rate of 2 °C·min^{-1} up to 600 °C. Copper weight expansion was also characterized by TGA at 400, 600, and 800 °C in air during 4 h at a heating rate of 1 °C·min^{-1}. Internal gas analysis (IGA) was performed to measure carbon and oxygen contents (Carbon-ISO15350, Oxygen-DIN EN 10276) in sintered specimens. Phosphorus content was measured by Inductively Coupled Plasma Optical Emission Spectrometry (ICP-OES, DIN 32633).

Thermal conductivities were measured on the sintering copper specimens and compared to a reference sample obtained from a copper powder pressed and sintered.

The thermal conductivity is calculated by using the following Eq. (2):

$$\lambda = Cp \times \rho \times \alpha \quad (2)$$

where λ [$W{\cdot}m^{-1}{\cdot}K^{-1}$] is the thermal conductivity, Cp [$J{\cdot}g^{-1}{\cdot}K^{-1}$] the heat capacity, ρ [$g{\cdot}cm^{-3}$] the material density and α [$mm^2{\cdot}s^{-1}$] the diffusivity.

The diffusivity was measured by a laser flash device (LFA Nanoflash Netzsch) on specimens with a diameter of 12.7 mm and a height between 2 to 3 mm required for high conductive material. The heat capacity of the Cu Ecka powder was measured with a calorimeter SETARAM C80 and fixed at 0.4 $J{\cdot}g^{-1}{\cdot}K^{-1}$ at 25 °C in the calculation of thermal conductivity. The density is measured using the Archimedes immersion method in anhydrous ethanol.

3 Results and discussion

3.1 Optical properties of copper

The curing behavior of photocurable formulation depends on the ability of the photoinitiator (PI) to absorb efficiently UV radiation. In formulations loaded with particles, the powder absorbs and/or diffuses the UV light leading to a decrease of the energy received by the PI. Low energy absorbed by the PI implies a low cured thickness of the printed layer. Figure 4 displays the measured total reflectivity and the calculated absorption of the Ecka copper powder. The absorption of copper particles decreases from 92 to 81% in the range of 250–500 nm. At 365 nm, the total reflectivity is about 13%, and the absorption 87%. The measurements performed are not able to make a distinction between absorption and diffusion contributions. However, these measurements show that copper is a non-UV-transparent material and it will be, therefore, affect the cured thickness of the metal formulation after UV exposure.

Besides, the optical index of copper at 365 nm includes a part related to light scattering n = 1.362 and another to absorption k = 1.962 [21]. This value confirms the fact that copper is non-transparent to UV. The particles will absorb a part of the UV light energy to the detriment of the photoinitiator in photosensitive resin, and a part will be diffused. The proportion of energy diffused and absorbed in an acrylate resin (refractive index n = 1.5) will be precisely described in further investigations.

3.2 UV curing behavior

The Cu Ecka powder was blended in photocurable resins noted F1, F2, F3, and F4. To limit the effect of the UV non-transparency of the Cu Ecka powder, formulations include PIs, known for their high reactivity at 365 nm, high efficiency in loaded and opaque formulations at a high rate of 5 wt.% to the organic resin.

In those conditions, Fig. 5 exhibits that cured thicknesses for the four formulations loaded at 60 vol.% of Cu are above the minimum target of 50 µm thickness. Cu F1 to F4 formulations are suitable to be printed by the DLP technology.

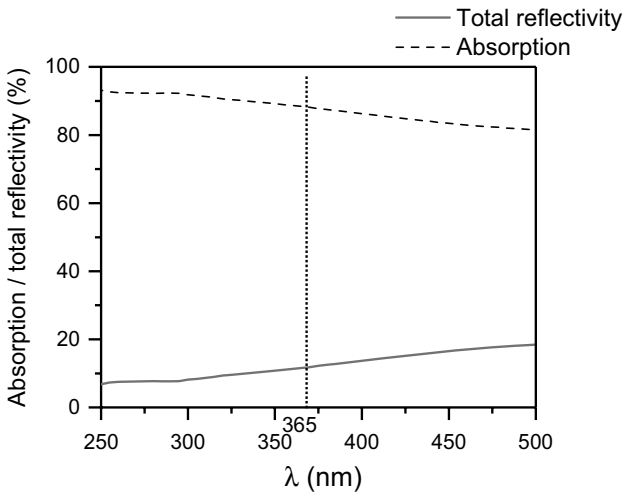

Fig. 4 Optical properties of copper ECKA powder poured in a quartz cell with an optical path length of 1 cm

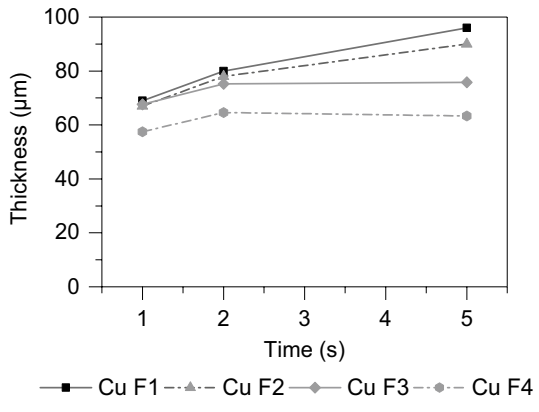

Fig. 5 Curing behavior of photocured resins loaded with 60 vol.% of copper Ecka powder Wavelength 365 nm and UV irradiance 88 $mW{\cdot}cm^{-2}$

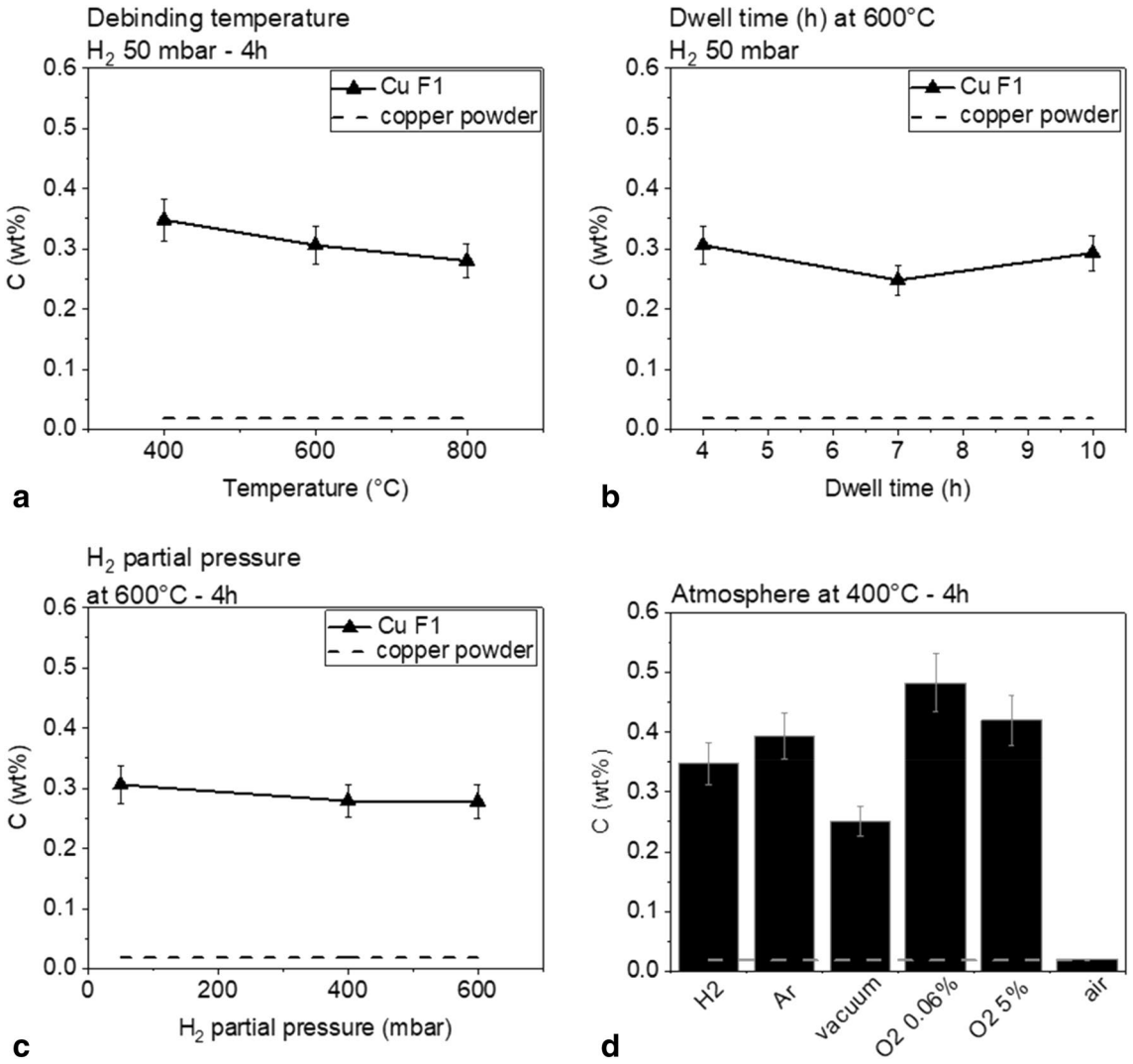

Fig. 6 Parameters affecting C content on Cu F1 green body cured by gamma irradiation **a** debinding temperature, **b** dwell time, **c** H_2 partial pressure and **d** atmosphere

3.3 Specimens cured by gamma irradiation

3.3.1 C&O contents after sintering at 980 °C

Once the photocuring formulation with a high copper loading rate and a curing behavior suitable to DLP technology developed, carbon and oxygen contents were studied on Cu F1 green body cured by gamma irradiation, then debinded in various conditions and sintered at 980 °C in hydrogen. Figure 6 illustrates the carbon contents on sintered copper cylinders and Cu Ecka powder (0.018 wt.%).

To debind and sinter in one thermal cycle and limit the thermal cost (atmosphere, furnaces), the debinding in the hydrogen of copper green bodies were firstly investigated.

In hydrogen, whatever debinding conditions (Fig. 6a–c debinding temperature, dwell time, and partial pressure) were, copper parts include a high carbon content of 0.25 wt.%. To decrease the carbon content and obtain copper metal, debinding atmospheres (Fig. 6d) like argon, vacuum, 600 ppm, and 5% O_2 in argon and air were assessed at 400 °C for 4 h. Carbon contents measured on copper parts in those debinding conditions are about 20 times higher (0.36 wt.%) than Cu Ecka powder except in air. Indeed, copper parts debinded in air and sintered in hydrogen reveal a carbon content of 0.019 wt.%, similar to the Cu powder.

Figure 7 exhibits the weight loss of the resins F1 to F4 in air and argon atmospheres and confirms previous observations. In the argon atmosphere, depending on the formulation, about 7% of char residues remain even at a temperature of 600 °C. In air, the resins are burned out. Air is considered a reactive atmosphere compared to

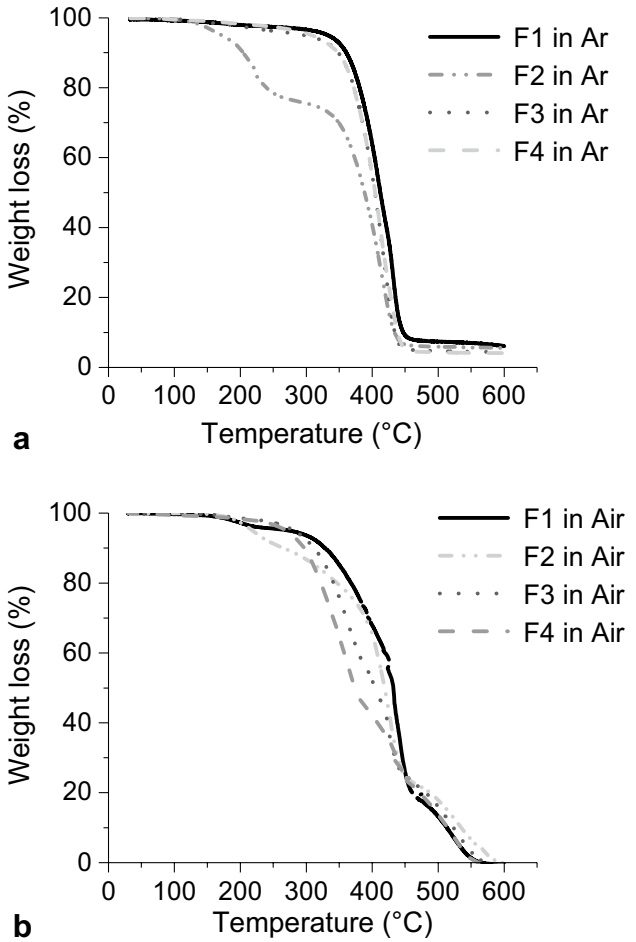

Fig. 7 TGA of the resins F1 to F4 **a** in an argon atmosphere and **b** in air atmosphere

argon; therefore, the char residue from resins reacts with the oxygen to form carbon monoxide (CO) and carbon dioxide (CO_2). The hydrogen atmosphere is also reactive as methane is expected to be emitted during resin degradation. However, according to the carbon content residue, the hydrogen atmosphere seems to be less effective than the oxidizing atmosphere to remove a photocured resin network.

In air, the copper is also oxidized, and an expansion accompanies this oxidation. The weight expansion of the copper measured by TGA is about 8, 14.4, and 16.8 wt.%, respectively, at 400, 600, and 800 °C. The debinding temperature is fixed at 400 °C to prevent cracks due to copper expansion.

However, at 400 °C, Fig. 7b shows that more than 40% of the resin is not completely degraded. A TGA analysis was performed at debinding conditions of 400 °C with a dwell time of 4 h in air. Depending on the formulation, between 10 and 19% of the resin remains. The nature of the char residues and/or the embrittlement of the organic network in air appears sensitive to the sintering atmosphere. Indeed the sintering in reactive hydrogen completes the degradation of the resin as the carbon content after sintering in the Cu F1 parts is similar to the Cu Ecka powder. At this thermal stage, the oxidized copper is also reduced in metal copper. However, the oxygen content is 3 times higher (0.085 wt.%) than the Cu Ecka powder.

Table 3 C and O contents (wt.%) of the Cu Ecka powder and Cu F1 to F4 formulations cured under gamma irradiation, debinded in air or argon 600 mbar at 400 °C - 4 h ramp 1 °C/min and, sintered at 980 °C - 4 h heating rate 3 °C min^{-1} in hydrogen 400 mbar (Cu F1-s to Cu F4-s)

	C (w.%)	O (wt.%)
Cu Ecka powder	0.018	0.028
Cu F1-s		
In argon	0.394	0.077
In air	0.019	0.084
Cu F2-s in air	0.022	0.063
Cu F3-s in air	0.018	0.054
Cu F4-s in air	0.013	0.077

Following this investigation on the Cu F1 formulation, the thermal cycle, including a debinding step in air and a sintering cycle in hydrogen, was applied to the Cu F2 to Cu F4 formulations.

Table 3 reports C&O contents of Cu F1 to Cu F4 formulations after a debinding in argon (only for Cu F1) and air at 400 °C followed by a sintering cycle in hydrogen at 980 °C (specimens are noted Cu Fx s). The values obtained are compared to the C&O contents of the Cu Ecka powder. The carbon rate measured for the four copper formulations are similar to the copper Ecka powder and demonstrates that the debinding in air is the most efficient atmosphere to degrade acrylate network. The oxygen content is 2 to 3.5 times higher than the one of the Cu Ecka powder and could affect final copper properties.

Figure 8 shows views of a green body copper cylinder, debinded in air (black specimen), and sintered in hydrogen, which completes the resin burning and the reduction of the copper parts. The shrinkage measured after sintering is about 19%.

3.3.2 O content and sintering temperature

To decrease the oxygen content in the final part, one strategy is to stay longer in hydrogen, in increasing the sintering temperature from 980 to 1050 °C. In those conditions, the oxygen content decreases significantly and achieves 0.067 wt.% at 1050 °C (Table 4). Another strategy, not reported in that work, should be to combine a high sintering temperature with a low heating rate in a hydrogen atmosphere.

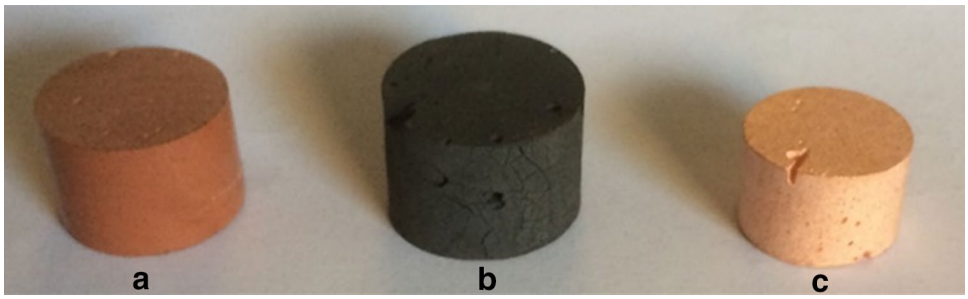

Fig. 8 Cu F1cylinders **a** gamma irradiation cured part, **b** debinded part at 400 °C for 4 h in air and **c** sintered part at 980 °C for 4 h in hydrogen at a partial pressure of 400 mbar

Table 4 C&O contents (wt.%) of the copper Ecka powder and the Cu F1 formulation cured under gamma irradiation, debinded in air and sintered in hydrogen at 980, 1030 and 1050 °C for 4 h at a heating rate of 3 °C·min^{-1}, and partial pressure of 400 mbar

	C (wt.%)	O (wt.%)
Cu Ecka powder	0.018	0.028
Sintering 3 °C·min^{-1} 980 °C	0.019	0.084
Sintering 3 °C·min^{-1} 1030 °C	0.017	0.077
Sintering 3 °C·min^{-1} 1050 °C	0.018	0.067

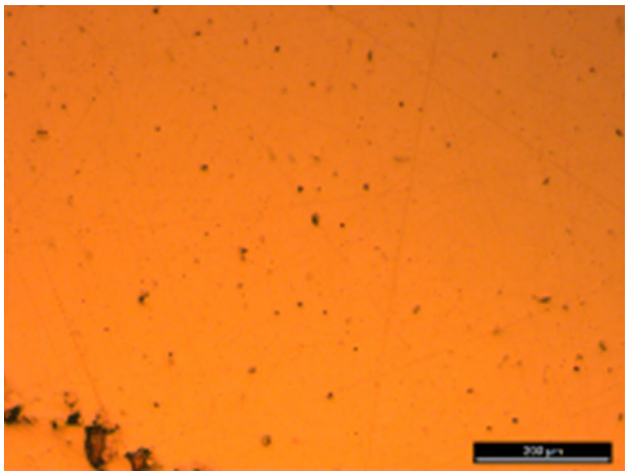

Fig. 9 Optical observation of Cu F4 s specimen cured by gamma irradiation and after debinding and sintering

3.3.3 Specimens observations and density

Densities were measured on the Cu F1 s to Cu F4 s specimens, and the Cu Ecka powder pressed and sintered (which correspond to our reference). The density of the reference is 97.8% ± 0.2 of the theoretical value of the DHP (deoxidized high phosphorus) copper (8.9 g·cm^{-3}) [20]. The density was calculated from the average of measurements done on three specimens and at three sintering temperatures (980, 1030, and 1050 °C). Densities of Cu F1 s to Cu F4 s were respectively 92 ± 3%, 82 ± 3%; 92 ± 1%, and 94 ± 1%. The optical observation of a copper specimen (Fig. 9) shows porosity homogeneously distributed, derived from the sintering process and coarser porosity, related to the shaping of the copper formulation. The copper paste has a high viscosity leading to an air trap in the copper formulation during the shaping in a tube. Accordingly, the density could be increased by improving the shaping method.

Density can also be affected by cracks from residual resin, stress related to the polymerization rate of the acrylate network, and/or the burnout of this polymerized organic media [22, 23]. Horizontal and vertical cracks are often observed for the Cu F1 s to Cu F3 s specimens, while no cracks are visible for the Cu F4 s (Fig. 10). As the temperature behavior (Fig. 7) of these resins appears to be similar, so one would expect similar observations regardless of the samples, which is not the case. Therefore if we consider that the gamma-ray polymerization of the resin is total, we can probably assume that the cracks are related to the stress in the organic network and, therefore, to the rate of polymerization of these resins. This point seems to be in line with the observations of samples Cu F3 s and Cu F4 s, the difference being due solely to a modification of the photoinitiator system.

3.3.4 Thermal conductivity

The conductivity measurement is determined from the density, the diffusivity and the heat capacity of the samples.

Figure 11 illustrates the thermal conductivity after a sintering cycle at 980, 1030, and 1050 °C in hydrogen. The λ of the reference is between 250 and 270 W·m^{-1}·K^{-1}, which is significantly lower than the pure copper (Cu-OFE 393 W·m^{-1}·K^{-1}) [24]. Cu Ecka powder includes phosphorus (0.025 wt.%) in that composition, which is known to reduce thermal conductivity drastically [20].

Cu F1 s (sintered) to Cu F3 s exhibit a low λ. Formulations include the BAPO photoinitiator, whose chemical formula is Phenylbis (2,4,6-trimethyl-benzoyl)phosphine oxide. The presence of phosphorus in BAPO leads to achieving 0.035 wt.% of phosphorus content in final copper parts. The low thermal conductivity is magnified by the low density of cylinders and the cracks observed on the

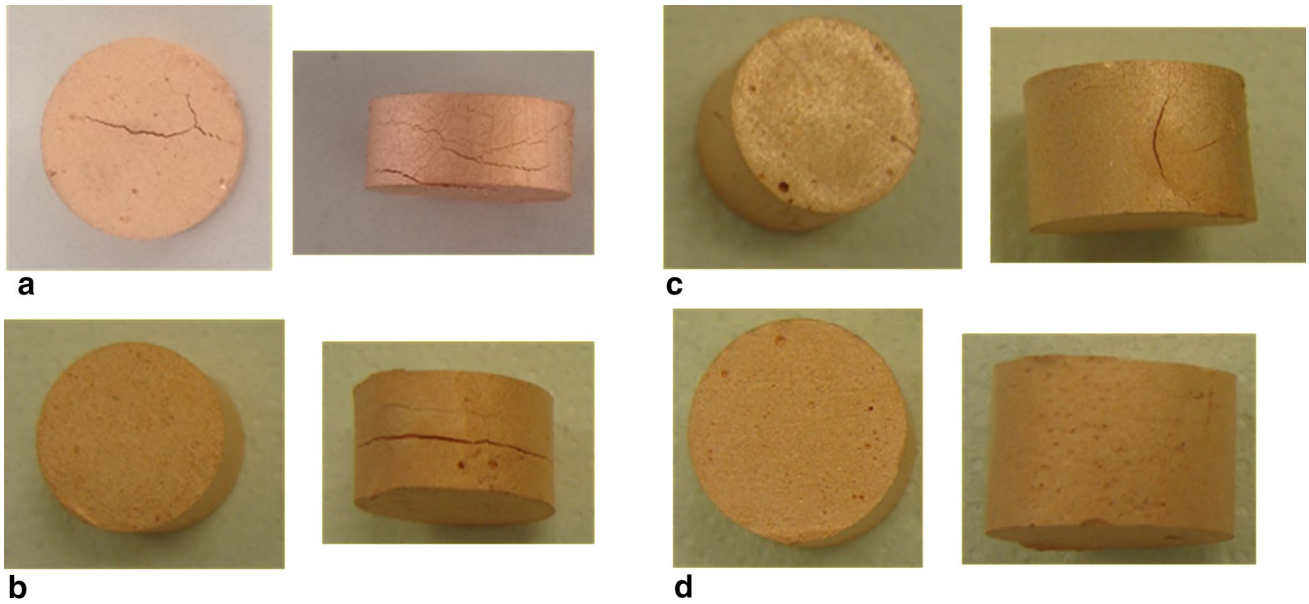

Fig. 10 Photos of the top view and side view of specimen cured by gamma-rays, debinding in air at 400 °C and sintering in hydrogen at 980 °C **a** Cu F1-s **b** Cu F2-s **c** Cu F3-s and **d** Cu F4-s

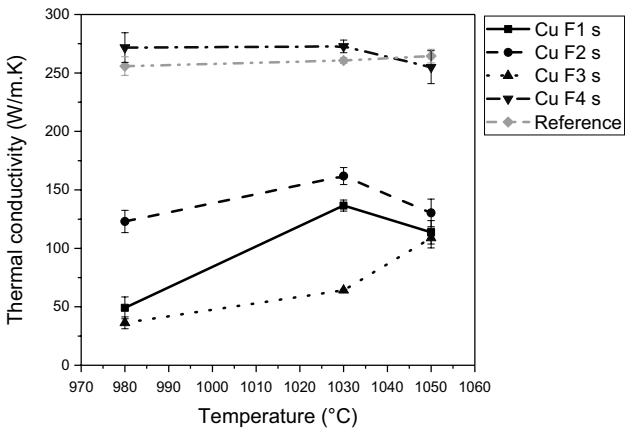

Fig. 11 Thermal conductivity of Cu F1 s to Cu F4 s (gamma irradiation) and Cu reference (pressed) after debinding in air and sintering in hydrogen at 980, 1030, and 1050 °C for 4 h at a heating rate of 3 °C·min^{-1} and partial pressure of 400 mbar

copper surface. However, it is not possible to distinguish the contribution of each of these inputs on the thermal conductivity in the current configuration.

Diffusivities measured on Cu F4 s specimens and Cu reference were respectively 82.7 ± 3.0 mm^2·s^{-1} and 77.2 ± 1.2 mm^2·s^{-1}. This result confirms the copper purity as the diffusivity is a constant of the material. The deviation of the results depends on the position in the LFA, the graphite layer quality, and the planarity of the specimen. Cu Fx s specimens were polished to meet the dimensional requirements of the LFA. In combining the density and the diffusivity, Cu F4 s exhibits a thermal conductivity similar to the reference. Besides, specimens have a composition in C&P elements similar to Cu Ecka powder.

The oxygen content is slightly higher, as previously commented, and does not appear to strongly affect the thermal conductivity.

3.4 DLP printed parts

Cu F1 formulation was chosen as a printing formulation related to its high UV curing behavior (Fig. 5). Cylinder copper parts for diffusivity measurement (12.6 mm diameter on 3 mm height) and gears (X = Y = 21.4 mm Z = 2.8 mm) were printed by the DLP process. According to the previous results, printed parts were debinded in air and sintered in hydrogen at 1050 °C. Cracks are observed as for specimens cured with gamma irradiation and then thermal treated.

C and O contents were measured on both geometries and reported in Table 5. The C and O contents of diffusivity parts printed by DLP appear similar to the parts cured by gamma irradiation.

The thermal conductivity of the printed parts was also calculated from the data of Table 5. The lower thermal conductivity of DLP parts (103 W·m^{-1}·K^{-1}) compared to the γ-ray cured specimens is mainly due to the material density. The density appears as a primary term in the thermal conductivity formula and indirectly in the diffusivity, which is the ability of the material to spread the heat. An increase of the porosity in the material leads to a decrease

Table 5 C&O contents (wt.%), diffusivity and density of the gear, DLP diffusivity part and gamma-ray cylinder (Cu F1 formulation printed, debinded in air and sintered in hydrogen at 1050 °C for 4 h at a heating rate of 3 °C min^{-1} and partial pressure of 400 mbar)

	C (wt.%)	O (wt.%)	Diffusivity ($mm^2 \cdot s^{-1}$)	Density (%)	Thermal conductivity ($W \cdot m^{-1} \cdot K^{-1}$)
DLP diffusivity part	0.018	0.062	32.0	90	103
Gear	0.017	0.022	–	–	–
Gamma-ray cylinder	0.018	0.067	35.7	93	118

in diffusivity. To improve the density of layer-wise printing parts, the influence of printing parameters should be investigated in detail.

Finally, many parameters affect thermal conductivity, as has been seen with the stress level in the cured resin, which can lead to cracks, the phosphorus rate, the density after the layer by layer process and the diffusivity measurement itself. Therefore, these results confirm the interest of the novel approach to investigate thermal cycles on photocurable formulation loaded with metal powder.

It is recognized that 3D printing is for conducting complex parts. Gears were printed in this objective (Fig. 12). The wall thicknesses of these objects are thin, allowing a better hydrogen diffusion in the copper parts during the sintering stage. The reduction of the copper oxide in metal is being easied. In those conditions, the C and O contents measured on gears point a similar composition to the Cu Ecka powder.

4 Conclusion

We have reported the development of photocurable formulations with copper particle contents of 60 vol.%, printable by digital light processing with layer thicknesses of at least 25 µm.

The fast gamma-rays approach was set up to cure quickly and enough samples for the four copper formulations to investigate thermal cycles and achieve copper parts. The thermal cycle investigations highlight that only a debinding of the cured resin in air at 400 °C for 4 h followed by a reduction of oxidized copper and sintering in hydrogen at 1050 °C allows to burn out the resin and reach a low carbon content (0.018 wt.%) similar to Cu raw powder. The O content reaches 0.067 wt.% based on Cu-F1 samples for 0.028 wt.% for raw copper powder in those conditions. The sintering cycle should be optimized to decrease the oxygen content. It may be considered to increase the time of the parts spent in hydrogen by adding dwells or reducing the heating rate.

The integrity of the specimen affects the final property and depends on the photocurable formulation and its stress after polymerization, the debinding cycle, which must be adapted to each formulation, and the contaminating elements. Phosphorus is a harmful element for the final properties of copper. In this study, phosphorus comes from the copper powder itself (0.025 wt.%), leading to a low thermal conductivity (250 and 270 $W \cdot m^{-1} \cdot K^{-1}$) compare to pure copper and also from the BAPO photoinitiator. BAPO-free Cu F4 s sample shows to achieving a λ close to the powder. In summary, to obtain copper parts with high thermal and electrical conductivity, it will be necessary to select powders without impurities harmful to copper (P, Ti, Co, Fe, As, Si) and to take particular care in the choice of the components of the photocurable resin.

Debinding and sintering conditions previously defined was applied to the copper DLP parts. C and O contents and thermal conductivity matched with the results obtained on samples cured by gamma irradiation. An oxygen content close to the initial copper powder is achievable with parts including thin wall thicknesses.

Fig. 12 Gear after DLP process, debinding in air at 400 °C for 4 h (black specimen) and sintering at 1050 °C for 4 h

Even if the cured networks obtained by gamma irradiation and by photocuring should be different, depending on the results, the approach based on fast gamma-ray curing appears to be promising to investigate thermal cycles of metals and ceramics printing by DLP.

The conditions of the thermal debinding and sintering cycles will have to be developed for each material. Indeed the use of air during the debinding process, even if it appears to be the most efficient atmosphere to burn out the resin network, is, however, not suitable for metals or non-oxide ceramics, which cannot be reduced during the sintering step.

Code availability Not applicable.

Compliance with ethical standards

Conflict of interest The authors declare that they have no known competing financial interests or personal relationships that could have appeared to influence the work reported in this paper.

Availability of data and material Not applicable.

References

1. Ahmed S, Hussain CM (2018) Green and sustainable advanced materials: applications. Wiley, Hoboken
2. Martin JD (2017) Exploring additive manufacturing processes for direct 3D printing of copper induction coils. In: ASME 2017 international mechanical engineering congress and exposition. American Society of Mechanical Engineers Digital Collection
3. Tran TQ, Chinnappan A, Lee JKY et al (2019) 3D printing of highly pure copper. Metals 9:756. https://doi.org/10.3390/met9070756
4. Kodama H (1981) Automatic method for fabricating a three-dimensional plastic model with photo-hardening polymer. Rev Sci Instrum 52:1770–1773. https://doi.org/10.1063/1.1136492
5. Colton J, Blair B (1999) Experimental study of post-build cure of stereolithography polymers for injection molds. Rapid Prototyp J 5:72–81. https://doi.org/10.1108/13552549910267452
6. Taormina G, Sciancalpore C, Messori M, Bondioli F (2018) Advanced resins for stereolithography: in situ generation of silver nanoparticles. AIP Conf Proc 1981:020065. https://doi.org/10.1063/1.5045927
7. Chartier T, Dupas C, Geffroy P-M et al (2017) Influence of irradiation parameters on the polymerization of ceramic reactive suspensions for stereolithography. J Eur Ceram Soc 37:4431–4436. https://doi.org/10.1016/j.jeurceramsoc.2017.05.050
8. Gentry SP, Halloran JW (2015) Light scattering in absorbing ceramic suspensions: effect on the width and depth of photopolymerized features. J Eur Ceram Soc 35:1895–1904. https://doi.org/10.1016/j.jeurceramsoc.2014.12.006
9. Zocca A, Colombo P, Gomes CM, Günster J (2015) Additive manufacturing of ceramics: issues, potentialities, and opportunities. J Am Ceram Soc 98:1983–2001. https://doi.org/10.1111/jace.13700
10. Lee JW, Lee IH, Cho D-W (2006) Development of micro-stereolithography technology using metal powder. Microelectron Eng 83:1253–1256. https://doi.org/10.1016/j.mee.2006.01.192
11. Vaneetveld G, Clarinval A-M, Dormal T et al (2008) Optimization of the formulation and post-treatment of stainless steel for rapid manufacturing. J Mater Process Technol 196:160–164. https://doi.org/10.1016/j.jmatprotec.2007.05.017
12. Zimbeck W, Pope M, Rice RW (1996) Microstructures and strengths of metals and ceramics made by photopolymer based rapid prototyping. In: 1996 international solid freeform fabrication symposium
13. Sano D, Kirihara S (2009) Fabrication of metal photonic crystals with graded lattice spacing by using micro-stereolithography. Mater Sci Forum 631–632:287–292. https://doi.org/10.4028/www.scientific.net/MSF.631-632.287
14. Kirihara S, Niki T, Kaneko M (2009) Terahertz wave behaviours in ceramic and metal structures fabricated by spatial joining of micro-stereolithography. J Phys Conf Ser 165:012082. https://doi.org/10.1088/1742-6596/165/1/012082
15. Matula RA (1979) Electrical resistivity of copper, gold, palladium, and silver. J Phys Chem Ref Data 8:1147–1298. https://doi.org/10.1063/1.555614
16. Hua D, Ge X, Tang J et al (2007) Controlled free-radical polymerization of methyl acrylate in the presence of a cyclic trithiocarbonate under γ-ray irradiation at low temperature. Eur Polym J 43:847–854. https://doi.org/10.1016/j.eurpolymj.2006.12.022
17. Wu Z, Zhang Z (2005) Controlled radical polymerization of acrylates by γ-irradiation in the presence of 1,1-diphenylethene. Radiat Phys Chem 74:331–337. https://doi.org/10.1016/j.radphyschem.2004.09.023
18. Hinczewski C, Corbel S, Chartier T (1998) Ceramic suspensions suitable for stereolithography. J Eur Ceram Soc 18:583–590. https://doi.org/10.1016/S0955-2219(97)00186-6
19. Dufaud O, Marchal P, Corbel S (2002) Rheological properties of PZT suspensions for stereolithography. J Eur Ceram Soc 22:2081–2092. https://doi.org/10.1016/S0955-2219(02)00036-5
20. Chapman D (2002) High conductivity copper for electrical engineering. http://copperalliance.it/uploads/2018/02/pub-122-hicon-copper-for-electrical-engineering.pdf
21. Mikhail Polyanskiy (2008–2020) Refractive index database. https://refractiveindex.info/. Accessed 15 June 2020
22. Bae C-J, Halloran JW (2011) Influence of residual monomer on cracking in ceramics fabricated by stereolithography: influence of residual monomer on cracking. Int J Appl Ceram Technol 8:1289–1295. https://doi.org/10.1111/j.1744-7402.2010.02578.x
23. Wang K, Qiu MB, Jiao C et al (2019) Study on defect-free debinding green body of ceramic formed by DLP technology. Ceram Int. https://doi.org/10.1016/j.ceramint.2019.09.237
24. Norm DIN EN 1976:2013 (2013) Copper and copper alloys—cast unwrought copper products Norm DIN EN 1976